

Self-assembly of colloid-cholesteric composites provides a possible route to switchable optical materials

K. Stratford*, O. Henrich*, J. S. Lintuvuori*,
M. E. Cates, D. Marenduzzo†

SUPA, School of Physics and Astronomy, The King's Buildings,
The University of Edinburgh, Edinburgh, EH9 3JZ, UK

* equally contributed to this work

† Corresponding author: dmarendu@ph.ed.ac.uk

Colloidal particles dispersed in liquid crystals can form new materials with tunable elastic and electro-optic properties. In a periodic ‘blue phase’ host, particles should template into colloidal crystals with potential uses in photonics, metamaterials, and transformational optics. Here we show by computer simulation that colloid/cholesteric mixtures can give rise to regular crystals, glasses, percolating gels, isolated clusters, twisted rings and undulating colloidal ropes. This structure can be tuned via particle concentration, and by varying the surface interactions of the cholesteric host with both the particles and confining walls. Many of these new materials are metastable: two or more structures can arise under identical thermodynamic conditions. The observed structure depends not only on the formulation protocol, but also on the history of an applied electric field. This new class of soft materials should thus be relevant to design of switchable, multistable devices for optical technologies such as smart glass and e-paper.

When spherical colloidal particles are mixed into a nematic liquid crystal, they disrupt the orientational order in the fluid and create defects (disclination lines) in the nematic close to their surfaces. To minimise the free energy

cost, it is generally advantageous for defects to be shared: therefore the colloidal particles have a generic tendency to aggregate. Such aggregates may further self-assemble into lines [1], 2D crystals [2], planar structures [3], or 3D amorphous glasses [4]. Besides being of fundamental interest to materials science, these structures may have tunable elastic and optical properties [5]. Hence they offer exciting prospects for applications as biosensors [6], or as new devices [7, 8].

But one may also choose to disperse colloidal particles in a cholesteric, rather than nematic, liquid crystal. The molecules making up this material are chiral, and this causes their average orientation (described by a director field) to rotate in space in a helical fashion, rather than remain uniform as in nematics. This typically creates a 1-dimensional periodic structure, called the cholesteric phase, whose wavelength is the pitch, p . The periodicity can however become fully three dimensional in the so-called blue phases (BPs) [9]. BPs arise because the director field can twist around more than one direction at once (see the cartoon in Supplementary Fig. 1). Such double twist regions (generally cylinders) are energetically favoured at high enough molecular chirality, but lead to geometric frustration because it is impossible to tile the whole 3D space with double twist cylinders without also introducing “disclination lines” (These are singular topological defects on which the director field is undefined.) In blue phases these disclination lines themselves either form a 3D periodic regular lattice (in so called BPI and BPII), or remain disordered (BPIII) [10]. BPs are stabilised by the tendency of chiral molecules to twist, but destabilised by the cost of forming topological defects (which locally diminish the molecular alignment). In conventional cholesteric materials [9] this balance is only achievable in a narrow temperature range of a few degrees, around the onset of liquid crystalline ordering. However, recent advances in formulation have widened this stability range enormously [11, 12, 13, 14]. Most recently, templated BPs with a stability range of -125 to 125°C have been reported [15], paving the way to applications of BPs in operational display devices.

Besides being remarkable materials in themselves, BPs offer significant promise as hosts for dispersing colloidal particles. Because BPs contain a disclination network even in the absence of particles, they can potentially template colloidal self-assembly. This was proved recently by simulations of BP-dispersed nanoparticles which exclude the surrounding liquid crystal but otherwise have negligible surface interaction with it (to give a so-called ‘weak anchoring’ regime) [16, 17]. Such particles are attracted to the discli-

nation network in BPs: by covering up the defect cores, the high elastic energy cost of those regions is avoided. The pre-existing order of the defect network then templates particles into a regular colloidal crystal of the same periodicity. Because this structure has a wavelength in the visible range, the resulting material should inherit (and probably enhance) the incomplete photonic bandgap of the parent blue phase, as exploited for instance in laser devices [12]; for related possibilities see [18].

A second compelling reason to study colloidal-BP composites is that, even without particles, BPs can show several competing metastable free energy minima, corresponding to different topologies of the defect network [19, 20], with a strong dependence on applied electric or magnetic fields [21]. Adding particles is likely to further enrich the free energy landscape, creating composites that might be promising candidates for bistable or multistable devices, in which energy is needed only to switch optical properties and not to maintain them. (This is the e-paper paradigm [22], and can lead to huge energy savings.) To explore such metastability, and switching strategies between states, we require multi-unit-cell, time-dependent simulations. These go beyond previous studies of colloidal-BP composites [17] but follow comparable simulations of pure BPs [10, 21, 23], and isolated and dimeric colloidal particles in cholesterics [24, 25].

The simulations presented here are representative of a liquid crystal blue phase with unit cell size in the range of 100–500 nm [9], and particles with a diameter of around 50 nm. The simulations address both the bulk structure, and the structure which forms when the colloidal dispersion is confined in a narrow sandwich of width comparable to the unit cell size [26]. It is seen that a wide variety of structure is possible, and may be influenced by parameters including the solid volume fraction, and the details of the anchoring at the colloid surface (and the at the surface of the confining walls). Further, evidence is found for metastable switching of this structure in an applied electric field. Details of the computational approach are set out in the Methods section, while simulation parameters are reported in the Supplementary Methods.

Results

Structure in bulk BPI. We show in Fig. 1 (**a–d**) the final state structures of four simulations in which we first equilibrated a stable BPI disclination network in bulk (with periodic boundary conditions) and then dispersed colloidal particles at random within it. Among dimensionless control parameters

are the particle solid volume fraction ϕ ($\phi = 1\%$ or 5%); the ratio $r = R/\lambda$ of particle radius to the BP lattice parameter λ (here $r \simeq 0.14$) and the ratio $w = WR/K$ where W is the anchoring strength of the cholesteric at the particle surface, and K is the elastic constant of the liquid crystal. The anchoring strength is defined such that $W > 0$ imparts a preferred orientation to the director field at the particle surface. This orientation can be either normal to the surface or in a plane tangential to the surface, a property related to surface chemistry in experimental systems. We choose $w = 0.23, 2.3$ which are within typical experimental range [4]. This parameter can be viewed as the ratio of the anchoring energy, WR^2 , to the elastic energy scale for distortion KR .

For a single colloidal particle in a nematic fluid, w controls the formation of a local topological defect at the particle surface [5], with weak distortion of the nearby fluid at small w . In the colloidal-BP system, w also plays a determining role in the final composite structure. When w is small (Fig. 1a and Fig. 1b; Supplementary Movies 1 and 2), the attraction of particles to the disclination lattice causes the lattice to become covered by particles, with little disruption of its long-range order. Thus a templated colloidal crystal is created, as first reported in [17]. Interestingly, the weak but finite anchoring apparently creates an elastic force between the colloidal particles which leads to very slow dynamics (Supplementary Fig. 4) and the formation of small colloidal lines within disclinations, especially for dilute samples (Fig. 1a). It seems likely that polymer-stabilised blue phases [11] work by a similar principle to this small w case, with a weak segregation of monomers towards the defect regions.

For large w (Fig. 1c and Fig. 1d; Supplementary Movies 3 and 4), the picture changes dramatically. Each colloidal particle now disrupts significantly the order of the nearby fluid, with defect formation close to its surface [5]. The resulting strong disruption of local liquid crystalline order around each particle leads now to a strong interparticle attraction. This restructures the disclination network completely, destroying the long range order of the original BPI topology. Most notably, particle aggregation favours the formation of defect junctions, where four disclinations meet. This structural motif is present in the unit cell of BPII rather than BPI (and also seen in the amorphous BPIII [10]). The particle clusters are disjoint at low volume fractions ($\phi \simeq 1\%$) but they interact elastically via the connecting disclinations. At larger ϕ , the aggregates join up to form a percolating colloidal cluster which essentially templates the disclinations rather than vice versa.

As colloidal-nematic composites [4], all the structures in Fig. 1 (**a–d**) should be soft solids, of nonzero elastic modulus G at low frequency. This contrasts with pure BPs, where $G = 0$ as the fluid can flow with a finite viscosity via permeation of molecules through a fixed defect lattice [27, 28]. We expect the structures in Fig. 1 (**a–c**) to be only weak gels, as here the defect network percolates but particle contacts do not. This is broadly similar to the cholesteric-nanoparticle gel reported in [29] (with $G < 1$ Pa). In contrast, the colloidal gel structure in Fig. 1**d** should be much more resistant mechanically, due to the formation of a thick percolating particle network. The structure is now akin to that of the self-quenched glass found in colloidal-nematic composites [4] at much higher volume fraction (over 20% as opposed to below 5% here), for which $G \sim 10^3$ Pa. This figure is consistent with an estimate obtained by comparing the mechanical properties of the network of defects stabilised by colloidal particles with those of rubber [30] for the relevant simulation parameters (see Supplementary Table 1).

A more practical protocol for including particles in a BPI phase is to disperse the particles at random in an isotropic phase, and then quenching this into the temperature range where BPI is stable. Here we know that, without particles, the kinetics can favour disordered (BPIII-like) intermediates which may be long lived or even metastable [23]. Fig. 1 (**e–h**) shows outcomes of such a quench protocol with the same parameter sets as in Fig. 1 (**a–d**). For small w , the particles again decorate the disclination lines, but are this time templated onto an amorphous network rather than an ordered one. Increasing the volume fraction (Fig. 1**f**) leads to a more even coverage with a better defined particle spacing. For large w , on the other hand, strong interparticle forces again dictate the self-assembly. At low concentrations, discrete particle clusters decorate an amorphous defect lattice (Fig. 1**g**) whereas at higher ϕ a percolating network of colloidal strands (the gel in Fig. 1**h**) is again seen. The structures in Fig. 1 (**a–h**) have been followed for ~ 20 ms (see Supplementary Fig. 4); they correspond to either very slowly evolving states or deep metastable minima (elastic interactions are of order KR and dwarf thermal motion, see Supplementary Fig. 4 and Ref. [5, 18]).

It may be possible to anneal the structures obtained via the quench route, although we have not attempted this in simulation. The results presented suggest that even when starting with colloidal particles randomly dispersed in an ordered blue phase, the particles are able to distort the structure (Fig. 1 **a,b**). This suggests that it would be difficult to identify a quench protocol which would lead to less, rather than more, disorder.

Structures in confined BPI. In display devices and other optical applications, it is typical for liquid crystals to be strongly confined (and subject to strong boundary effects), in contrast to the bulk geometries considered above. We therefore next describe how colloidal suspensions self assemble in thin sandwiches (thickness $h = 1.75\lambda$), whose confining walls can favour either tangential (planar degenerate) or normal (homeotropic) orientation of the director field. For simplicity we here impose one or the other as a strict boundary condition.

Fig. 2 (**a–d**) shows the case of normal wall anchoring on varying ϕ and w . We quench from the isotropic to the ordered phase as was done in Fig. 1 (**e–h**), and again find a metastable, amorphous disclination network (see Supplementary Methods). The resulting colloidal-cholesteric composites are somewhat similar to those seen in the bulk: for small w the particles are templated by the network (Fig. 2**a,b**), whereas for large w we observe isolated clusters (Fig. 2**c**) and percolated colloidal gels (Fig. 2**d**), for $\phi = 1\%$ and 4% respectively. There are, however, significant effects of the confining walls. First, the normal anchoring at the wall recruits particles there, giving (for the chosen h) a density enhancement of the colloid particles at both walls (see side-views in Fig. 2**a–d**). Second, the clusters formed at large w are themselves anisotropic with an oblate habit. These clusters are similar to those reported experimentally for large colloid particles in a cholesteric (but non-BP) host [31].

Fig. 2 (**e–h**) shows comparable simulations for planar wall anchoring. Without colloidal particles, planar anchoring results in a regular cholesteric helix, with axis perpendicular to the boundary walls. This twisted texture develops via a set of defect loops, which shrink and disappear to leave a defect-free sample. However, dispersing particles with small w arrests the loop shrinking process, stabilising twisted rings (Fig. 2**e**) at small ϕ , and more complicated double-stranded structures at larger ϕ (Fig. 2**f**). For larger w , we observe thick colloidal “ropes” about 5 particles across (Fig. 2**g,h**). These ropes undulate to follow the chiral structure of the underlying fluid. On increasing the density they develop branch points and finally again approach a percolating gel morphology. Note that planar wall anchoring is incompatible with the normal anchoring on the colloidal particles (for $w > 0$), which are thus repelled from both walls (see the side views in Fig. 2**e–h**).

The degree of similarity between the bulk and confined structures is somewhat masked by the local change in particle density in the confined case. If one allows for this, Figs. 1 and 2 show the individual structural motifs are

actually rather similar: templated lines for weak anchoring and clusters for strong anchoring.

Switching in electric field. An interesting question, relevant for applications to devices, is whether these structures can be modified, or switched, with electric fields. Fig. 3 addresses this question, starting from amorphous blue phase III, this time at a higher chirality. Dispersing colloidal particles in this network results in the particle occupying the available nodes, where the order parameter is low (Fig. 3a; Supplementary Movie 5). Applying a high enough field along the x direction leads to a switching to a new phase, where colloidal arrays fit within a network with distorted hexagonal cells (Fig. 3b and Supplementary Fig. 7; Supplementary Movie 6). Remarkably, upon field removal this honeycomb structure does not find its way back to the configuration before switching on the field, but gets stuck into a metastable structure (Supplementary Fig. 7), with residual anisotropy along the field switching direction. Cycling the field along the x and y directions leads to distinct metastable structures, which are retained after field removal (Supplementary Fig. 8 and Fig. 9). We note that for the fluid parameters used here, the field induced changes are irreversible with the weakly anchoring colloid particles. The mesophase without colloid particles undergoes a reversible ordering transition [10]; the reversibility is retained in the presence of particles only if their anchoring is very weak.

Discussion

The surprising wealth of colloidal-BP composites obtained in Figs. 1-3 is the complex consequence of a simple competition between two self-assembly principles. First, blue phases provide a three-dimensional template onto which colloidal particles are attracted so as to reduce the elastic stresses arising at the disclination cores [17]. Second, colloidal intrusions in a liquid crystal raise the free energy locally; sharing this cost creates a generic tendency to aggregate into clusters [4]. Which of these factors dominates depends on w , a dimensionless measure of the anchoring strength of the director field at the colloidal surface. For $w \ll 1$, the templating principle dominates. Colloidal crystals, gels or twisted rings can then arise. For $w \gg 1$, interparticle attractions defeat the templating tendency, and we predict disconnected aggregates, percolating gels, or helical colloidal ropes. In both cases, control is offered by the process route, colloidal concentration, and the anchoring conditions at sample walls. We have also shown that electric fields can be used to switch between metastable states, providing a possible route to future

multistable device applications.

How do these simulations relate to experiment? Several authors have used nanoparticles in the context of stabilising BPs [32, 33]. These nanoparticles are typically a few nanometres in size, in which case stabilisation is explained by the mechanism of defect removal. Experiments suggest this mechanism is also relevant for larger particles in the range of 40–70 nm [34], which is consistent with the current simulations. However, the mechanism is observed to be less efficient for particles above 100 nm, where particles may start to disrupt longer-range liquid crystal order [34]. While the field of self-assembly with nanoparticles is relatively new [35], nanoparticles have also been used in both nematic [36] and chiral liquid crystals [37] as host fluid templates. The variation of structure seen in our simulations suggest that some careful characterisation of parameters such as surface anchoring of particles (which are often stabilised, or even functionalised with surface ligands), together with those associated with any confining surfaces or interfaces, is required to understand the final structure and to be able to reproduce it with a given experimental protocol. The identification of a model system which could allow unambiguous comparison between experimental systems and simulation would be extremely useful. Such a system might adopt particles of diameter in the range 50 nm or above, which allows a coarse-grained simulation approach of the type used here to be adopted, which can then capture the large-scale structure required to compare with experiment. In the same vein, detailed surface chemistry is difficult to represent in coarse-grained simulations, so heavily functionalised particles might be avoided.

We have not explored in this work switchability by flow [38], but this could again be inherited from the underlying BP dynamics [19, 28], in which case the same materials may also be relevant to the emerging technology of optofluidics [39].

Methods

Here, the simulation method is described. Note that all quantities are expressed in simulation units. Details of the simulation parameters, and their mapping to physical units, may be found in Supplementary Table 1 and the Supplementary Methods.

Thermodynamics. The thermodynamics of the cholesteric liquid crystal can be described by means of a Landau-de Gennes free energy functional \mathcal{F} ,

whose density is written as f :

$$\mathcal{F}[\mathbf{Q}] = \int d^3\mathbf{r} f(\mathbf{Q}(\mathbf{r})). \quad (1)$$

This free energy density $f = f(\mathbf{Q})$ may be expanded in powers of the order parameter \mathbf{Q} and its gradients; \mathbf{Q} is a traceless and symmetric tensor which is denoted from now on in subscript notation as $Q_{\alpha\beta}$. The largest eigenvalue q and corresponding eigenvector n_α of $Q_{\alpha\beta}$ describe the local strength and major orientation axis of molecular order. The theory based on the tensor $Q_{\alpha\beta}$, rather than a theory based solely on the director field $n_\alpha(\mathbf{r})$, allows treatment of disclinations (defect lines) in whose cores n_α is undefined.

Explicitly, the free energy density is:

$$\begin{aligned} f(Q_{\alpha\beta}) = & \frac{1}{2}A_0 \left(1 - \frac{1}{3}\gamma\right) Q_{\alpha\beta}^2 - \frac{1}{3}A_0\gamma Q_{\alpha\beta}Q_{\beta\gamma}Q_{\gamma\alpha} + \frac{1}{4}A_0\gamma(Q_{\alpha\beta}^2)^2 \\ & + \frac{1}{2}K(\varepsilon_{\alpha\gamma\delta}\partial_\gamma Q_{\delta\beta} + 2q_0Q_{\alpha\beta})^2 + \frac{1}{2}K(\partial_\beta Q_{\alpha\beta})^2. \end{aligned} \quad (2)$$

Here, repeated indices are summed over, while terms of the form $Q_{\alpha\beta}^2$ should be expanded to read $Q_{\alpha\beta}Q_{\alpha\beta}$; $\varepsilon_{\alpha\gamma\delta}$ is the permutation tensor. The first three terms are a bulk free energy density whose overall scale is set by A_0 (discussed further below); γ is a control parameter related to a reduced temperature. Varying the latter in the absence of chiral terms ($q_0 = 0$) gives an isotropic-nematic transition at $\gamma = 2.7$ with a mean-field spinodal instability at $\gamma = 3$.

The remaining two terms of the free energy density in Eq. 2 describe distortions of the order parameter field. In theoretical work and when describing a generic rather than a specific system, it is conventional [9, 40] to assume that splay, bend and twist deformations of the director are equally costly, that is, there is a single elastic constant K . The parameter q_0 is related to the helical pitch length p via $q_0 = 2\pi/p$, describing one full turn of the director in the cholesteric phase.

There are two dimensionless numbers, which are commonly referred to as κ , the chirality, and τ , the reduced temperature [9] which can be used to characterise the system. In terms of the parameters in the free energy density, these are:

$$\tau = \frac{27(1 - \gamma/3)}{\gamma} \quad (3)$$

$$\kappa = \sqrt{\frac{108 K q_0^2}{A_0 \gamma}}. \quad (4)$$

If the free energy density Eq. 2 is made dimensionless, τ appears as prefactor of the term quadratic in $Q_{\alpha\beta}$, whereas κ quantifies the ratio between bulk and gradient free energy terms. The chirality and reduced temperature may be used to characterise an equilibrium phase diagram of the blue phases in bulk cholesteric liquid crystals [9, 21].

The effect of an electric field can be modelled by including the following term in the bulk free energy density:

$$-\frac{\epsilon_a}{12\pi}E_\alpha Q_{\alpha\beta}E_\beta, \quad (5)$$

where E_α are the components of the electric field, and ϵ_a (here assumed positive) is the dielectric anisotropy of the liquid crystal. The strength of the electric field is quantified via one further dimensionless number

$$\mathcal{E}^2 = \frac{27\epsilon_a}{32\pi A_0\gamma}E_\alpha E_\alpha. \quad (6)$$

The quantity \mathcal{E} is known as the reduced field strength.

Surface free energy. In addition to the fluid free energy density $f(Q_{\alpha\beta})$, a surface free energy density is also present to represent the energetic cost of anchoring at a solid surface. In the case of normal anchoring, the surface free energy density (per unit area) is

$$f_s(Q_{\alpha\beta}, Q_{\alpha\beta}^0) = \frac{1}{2}W(Q_{\alpha\beta} - Q_{\alpha\beta}^0)^2, \quad (7)$$

where $Q_{\alpha\beta}^0$ is the preferred order parameter tensor at the solid surface, and W is a constant determining the strength of the anchoring. In the case of planar anchoring, a slightly more complicated expression is required to allow for degeneracy (see, e.g., [44]). The determination of $Q_{\alpha\beta}^0$ for normal and planar anchoring is discussed below. For a colloidal particle of radius R , the strength of the surface anchoring compared which the bulk fluid elastic constant may be quantified by the dimensionless parameter WR/K . For small values of this parameter, the presence of a particle surface should have little impact on the local fluid LC ordering.

Dynamics of the order parameter. A framework for the dynamics of liquid crystals is provided by the Beris-Edwards model [41], in which the time evolution of the tensor order parameter obeys

$$(\partial_t + u_\nu\partial_\nu)Q_{\alpha\beta} - S_{\alpha\beta} = \Gamma H_{\alpha\beta}. \quad (8)$$

In the absence of flow, Eq. 8 describes a relaxation towards equilibrium on a timescale determined by a collective rotational diffusion constant Γ . This relaxation is driven by the molecular field $H_{\alpha\beta}$, which is the functional derivative of the free energy with respect to the order parameter [41]:

$$H_{\alpha\beta} = -\frac{\delta\mathcal{F}}{\delta Q_{\alpha\beta}} + \frac{1}{3}\delta_{\alpha\beta}\text{Tr}\left(\frac{\delta\mathcal{F}}{\delta Q_{\alpha\beta}}\right). \quad (9)$$

The tensor $S_{\alpha\beta}$ in Eq. 8 completes the material derivative for rod-like molecules [41]. It couples the order parameter to the symmetric and anti-symmetric parts of the velocity gradient tensor $W_{\alpha\beta} \equiv \partial_\beta u_\alpha$. The symmetric part $A_{\alpha\beta}$ and the antisymmetric part $\Omega_{\alpha\beta}$ are defined as

$$A_{\alpha\beta} = \frac{1}{2}(W_{\alpha\beta} + W_{\beta\alpha}), \quad (10)$$

and

$$\Omega_{\alpha\beta} = \frac{1}{2}(W_{\alpha\beta} - W_{\beta\alpha}). \quad (11)$$

This full coupling term is then

$$\begin{aligned} S_{\alpha\beta} &= (\xi A_{\alpha\nu} + \Omega_{\alpha\nu})(Q_{\nu\beta} + \frac{1}{3}\delta_{\nu\beta}) + (Q_{\alpha\nu} + \frac{1}{3}\delta_{\alpha\nu})(\xi A_{\nu\beta} - \Omega_{\nu\beta}) \\ &- 2\xi(Q_{\alpha\beta} + \frac{1}{3}\delta_{\alpha\beta})Q_{\nu\nu}W_{\nu\nu}. \end{aligned} \quad (12)$$

Here, ξ is a material-dependent that controls the relative importance of rotational and elongational flow for molecular alignment, and determines in practice how the orientational order responds to a local shear flow. In all cases, the value used here is $\xi = 0.7$, which is within the ‘flow aligning’ regime, where molecules align at a fixed angle (the Leslie angle) to the flow direction in weak simple shear [40]. The value of the collective rotational diffusion used in all simulations is $\Gamma = 0.5$ in simulation units.

Hydrodynamics. The momentum evolution obeys a Navier-Stokes equation driven by the divergence of a generalised stress $P_{\alpha\beta}$:

$$\rho \partial_t u_\alpha + \rho u_\beta \partial_\beta u_\alpha = \partial_\beta P_{\alpha\beta}. \quad (13)$$

The pressure tensor $P_{\alpha\beta}$ is, in general, asymmetric and includes both viscous and thermodynamic components:

$$\begin{aligned} P_{\alpha\beta} &= -p_0\delta_{\alpha\beta} + \eta\{\partial_\alpha u_\beta + \partial_\beta u_\alpha\} \\ &- \xi H_{\alpha\gamma} \left(Q_{\gamma\beta} + \frac{1}{3}\delta_{\gamma\beta}\right) - \xi \left(Q_{\alpha\gamma} + \frac{1}{3}\delta_{\alpha\gamma}\right) H_{\gamma\beta} \\ &+ 2\xi \left(Q_{\alpha\beta} + \frac{1}{3}\delta_{\alpha\beta}\right) Q_{\gamma\nu} H_{\gamma\nu} - \partial_\alpha Q_{\gamma\nu} \frac{\delta\mathcal{F}}{\delta\partial_\beta Q_{\gamma\nu}} \\ &+ Q_{\alpha\gamma} H_{\gamma\beta} - H_{\alpha\gamma} Q_{\gamma\beta}. \end{aligned} \quad (14)$$

A lattice Boltzmann (LB) flow solver is used, where the isotropic pressure p_0 and viscous terms are managed directly by the solver (as in a simple Newtonian fluid, of viscosity η), whereas the divergence of the remaining terms is treated as a local force density on the fluid. In all simulations reported the mean fluid density $\rho = 1$ and the viscosity $\eta = 0.01$ (simulations in confined geometry also used enhanced bulk viscosity $\zeta = 10\eta$ to ensure numerical stability).

Surface boundary conditions for particles. Hydrodynamic boundary conditions for solid objects are handled via the lattice Boltzmann solver. In particular, the standard method of bounce-back on links is used for both particles and confining walls [42, 43]. Boundary conditions for the order parameter are set out in [45].

In all the simulations reported here the preferred orientation of the director field at the particle surface is normal to the surface. The required nematic director at the particle surface in a given location \hat{n}_α^0 may then be determined from geometry alone, and a preferred order parameter $Q_{\alpha\beta}^0$ is computed via

$$Q_{\alpha\beta}^0 = q^0(\hat{n}_\alpha^0\hat{n}_\beta^0 - \frac{1}{3}\delta_{\alpha\beta}). \quad (15)$$

The magnitude of surface order q^0 is set by

$$q^0 = \frac{2}{3} \left(\frac{1}{4} + \frac{3}{4} \sqrt{1 + (8/3\gamma)} \right) \quad (16)$$

which corresponds to the bulk order in a defect-free nematically ordered sample [46] (this is also very close to the value of the order parameter in a cholesteric or in a blue phase away from disclinations).

In all simulations the colloidal (hard sphere) radius is $R = 2.3$. To prevent particles overlapping at the hard sphere radius, an additional short range soft potential is included. This takes the form of $V(h) = \epsilon(\sigma/h)$ where h is the surface to surface separation. The parameters are $\epsilon = 0.0004$ and $\sigma = 0.1$ in simulation units. Both potential and resulting force are smoothly matched to zero at a cut-off distance of $h_c = 0.25$ simulation units.

Surface boundary conditions for walls. The confining solid walls, which are flat and stationary, have the same normal boundary condition as at the particle surface. In addition, degenerate planar anchoring is applied at the walls, where the preferred nematic director may adopt any orientation parallel to the surface. The preferred direction is determined explicitly by pro-

jecting the local fluid order parameter to the plane of the wall [44]. Eq. 15 and Eq. 16 are then used as before.

To prevent the particles being forced into the wall, a correction to the lubrication force on the colloidal particle is added for very low particle surface to wall surface separations $h < 0.5$ lattice spacing. The correction is based on the analytic expression for the lubrication between a sphere and a flat surface.

References

- [1] Ravnik, M., et al., Entangled nematic colloidal dimers and wires, *Phys. Rev. Lett.* **99**, 247801 (2007).
- [2] Musevic, I., Skarabot, M., Tkalec, U., Ravnik, M., and Zumer, S., Two-dimensional nematic colloidal crystals self-assembled by topological defects, *Science* **313**, 954–958 (2006).
- [3] Araki, T., and Tanaka, H., Colloidal aggregation in a nematic liquid crystal: topological arrest of particles by a single-stroke disclination line, *Phys. Rev. Lett.* **97**, 127801 (2006).
- [4] Wood, T.A., Lintuvuori, J.S., Schofield, A.B, Marenduzzo, D., and Poon, W.C.K., A self-quenched defect glass in a colloid-nematic liquid crystal composite, *Science* **333**, 79–83 (2011).
- [5] Stark, H., Physics of colloidal dispersions in nematic liquid crystals, *Phys. Rep.* **351**, 387–474 (2001).
- [6] Lin, I.H., et al., Endotoxin-induced structural transformations in liquid crystalline droplet, *Science* **332**, 1297–1300 (2011).
- [7] Chari, K., Rankin, C.M., Johnson, D.M, Blanton, T.N., and Capurso, R.G., Single-substrate cholesteric liquid crystal displays by colloidal self-assembly, *Appl. Phys. Lett.* **88**, 043502 (2006).
- [8] Araki, T., Buscaglia, M., Bellini, T., and Tanaka, H., Memory and topological frustration in nematic liquid crystals confined in porous materials, *Nat. Mat.* **10**, 303–309 (2011).
- [9] Wright, D.C., and Mermin, N.D., Crystalline liquids: the blue phases, *Rev. Mod. Phys.* **61**, 385–432 (1989).
- [10] Henrich, O., Stratford, K., Cates, M.E., and Marenduzzo, D., Structure of blue phase III of cholesteric liquid crystals, *Phys. Rev. Lett.* **106**, 107802 (2011).
- [11] Kikuchi, H., Yokota, M., Hisakado, Y., Yang, H., and Kajiyama, T., Polymer-stabilized liquid crystal blue phases, *Nat. Mat.* **1**, 64–68 (2002).

- [12] Cao, W.Y., Munoz, A., Palffy-Muhoray, P., and Taheri, B., Lasing in a three-dimensional photonic crystal of the liquid crystal blue phase II, *Nat. Mat.* **1**, 111–113 (2002).
- [13] Coles, H.J., and Pivnenko, M.N., Liquid crystal ‘blue phases’ with a wide temperature range, *Nature* **436**, 997–1000 (2005).
- [14] Ge, Z.B., Gauza, S., Jiao, M.Z., Xianyu, H.Q., and Wu, S.T., Electro-optics of polymer-stabilized blue phase liquid crystal displays, *Appl. Phys. Lett.* **94**, 101104 (2009).
- [15] Castles, F., et al., Blue-phase templated fabrication of three-dimensional nanostructures for photonic applications, *Nat. Mat.* **11**, 599–603 (2012).
- [16] Ravnik, M., Alexander, G.P., Yeomans, J.M., and Zumer, S., Mesoscopic modelling of colloids in chiral nematics, *Faraday Discuss.* **144**, 159–169 (2010).
- [17] Ravnik, M., Alexander, G.P., Yeomans, J.M., and Zumer, S., Three-dimensional colloidal crystals in liquid crystalline blue phases, *Proc. Natl. Acad. Sci. USA* **108**, 5188–5192 (2011).
- [18] Lavrentovich, O.D., Liquid crystals, photonic crystals, metamaterials and transformation optics, *Proc. Natl. Acad. Sci. USA* **108**, 5143–5144 (2011).
- [19] Tiribocchi, A., Gonnella, G., Marenduzzo, D., Orlandini, E., and Salvatore, F., Bistable defect structures In blue phase devices, *Phys. Rev. Lett.* **107**, 237803 (2011).
- [20] Fukuda, J.-I., and Zumer, S., Quasi-two-dimensional Skyrmion lattices in a chiral nematic liquid crystal, *Nat. Commun.* **2**, 246 (2011).
- [21] Henrich, O., Marenduzzo, D., Stratford, K., and Cates, M.E., Thermodynamics of blue phases in electric fields, *Phys. Rev. E* **81**, 031706 (2010).
- [22] Heikenfeld, J., Drzaic, P., Yeo, J.S., and Koch, T., A critical review of the present and future prospects for electronic paper, *J. Soc. Inf. Display* **19**, 129–156 (2011).

- [23] Henrich, O., Stratford, K., Marenduzzo, D., and Cates, M.E., Ordering dynamics of blue phases entails kinetic stabilization of amorphous networks, *Proc. Natl. Acad. Sci. USA* **107**, 13212–13215 (2010).
- [24] Lintuvuori, J.S., Stratford, K., Cates, M.E., and Marenduzzo, D., Colloids in cholesterics: size-dependent defects and non-Stokesian microrheology, *Phys. Rev. Lett.* **105**, 178302 (2010).
- [25] Lintuvuori, J.S., Stratford, K., Cates, M.E., and Marenduzzo, D., Self-assembly and nonlinear dynamics of dimeric colloidal rotors in cholesterics, *Phys. Rev. Lett.* **107**, 267802 (2011).
- [26] Ravnik, M., Fukuda, J.-I., Yeomans, J.M., and Zumer, S., Confining blue phase colloids to thin layers, *Soft Matter* **7**, 10144–10150 (2011).
- [27] Helfrich, W., Capillary flow of cholesteric and smectic liquid crystals, *Phys. Rev. Lett.* **23**, 372–374 (1969).
- [28] Dupuis, A., Marenduzzo, D., Orlandini, E., and Yeomans, J.M., Rheology of cholesteric blue phases, *Phys. Rev. Lett.* **95**, 097801 (2005).
- [29] Zapotocky, M., Ramos, L., Poulin, P., Lubensky, T.C., and Weitz, D.A., Particle-stabilized defect gel in cholesteric liquid crystals, *Science* **283**, 209–212 (1999).
- [30] Ramos, L., Zapotocky, M., Lubensky, T.C., and Weitz, D.A., Rheology of defect networks in cholesteric liquid crystals, *Phys. Rev. E* **66** 031711 (2002).
- [31] Hijnen, N., Wood, T.A., Wilson, D., and Clegg, P.S., Self-organization of particles with planar surface anchoring in a cholesteric liquid crystal, *Langmuir* **26**, 13502–13510 (2010).
- [32] Yoshida, H., et al., Nanoparticle-stabilized cholesteric blue phases, *Appl. Phys. Express*, **2**, 121501 (2009).
- [33] Karatairi, E., et al., Nanoparticle-induced widening of the temperature range of liquid-crystalline blue phases, *Phys. Rev. E* **81**, 041703 (2010).
- [34] Dierking, I., et al., Stabilising liquid crystalline blue phases, *Soft Matter* **8**, 4355–4362 (2012).

- [35] Draper, M., et al. Self-assembly and shape morphology of liquid crystalline gold metamaterials, *Adv. Func. Mat.*, **21** 1260–1278 (2011).
- [36] Milette, J., et al., Reversible long-range network formation in gold nanoparticle-nematic liquid crystal composites, *Soft Matter*, **8**, 173–179 (2012).
- [37] Cordoyiannis, G., et al., Different modulated structures of topological defects stabilized by adaptive targeting nanoparticles, *Soft Matter* **9**, 3956–3964 (2013).
- [38] Henrich, O., Stratford, K., Coveney, P.V., Cates, M.E., and Marenduzzo, D., Rheology of cubic blue phases, *Soft Matter* 10243–10256 (2013).
- [39] Psaltis, D., Quake, S.R., Yang, C., Developing optofluidic technology through the fusion of microfluidics and optics *Nature* **442**, 381–386 (2006).
- [40] de Gennes, P.-G., and Prost, J., *The Physics of Liquid Crystals* (Clarendon Press, 1995).
- [41] Beris, A.N., and Edwards, B.J., *Thermodynamics of Flowing Systems with Internal Microstructure* (Oxford University Press, 1994).
- [42] Ladd, A.J.C., *J. Fluid Mech.* Numerical simulation of particulate suspensions via a discretized Boltzmann equation. Part 1. Theoretical foundation, **271**, 285–309 (1994).
- [43] Nguyen, N.-Q., and Ladd, A.J.C., Lubrication corrections for lattice Boltzmann simulations of particle suspensions, *Phys. Rev. E* **66** 046708 (2002).
- [44] Fournier, J.-B., and Galatola, P., Modeling planar degenerate wetting and anchoring in nematic liquid crystals, *Europhys. Lett.* **72**, 403–409 (2005).
- [45] Lintuvuori, J.S., Marenduzzo, D., Stratford, K., and Cates, M.E., Colloids in liquid crystals: a lattice Boltzmann study, *J. Mater. Chem.* **20**, 10547–10552 (2010).

- [46] Denniston, C., Orlandini, E., and Yeomans, J.M., Lattice Boltzmann simulations of liquid crystal hydrodynamics, *Phys. Rev. E* **63**, 056702 (2001).

Acknowledgements

We acknowledge support by UK EPSRC grants EP/J007404/1 (KS and JSL), EP/G036136/1 (OH), and EP/I030298/1 (KS and JSL). MEC is supported by the Royal Society. We thank both Hector and PRACE for computational resources.

Author Contributions

KS, OH and JSL contributed to the code base for simulation and performed simulations. All authors helped to analyse the results and write the manuscript.

Additional Information

Competing financial interests: The authors declare no competing financial interests.

Blank page.

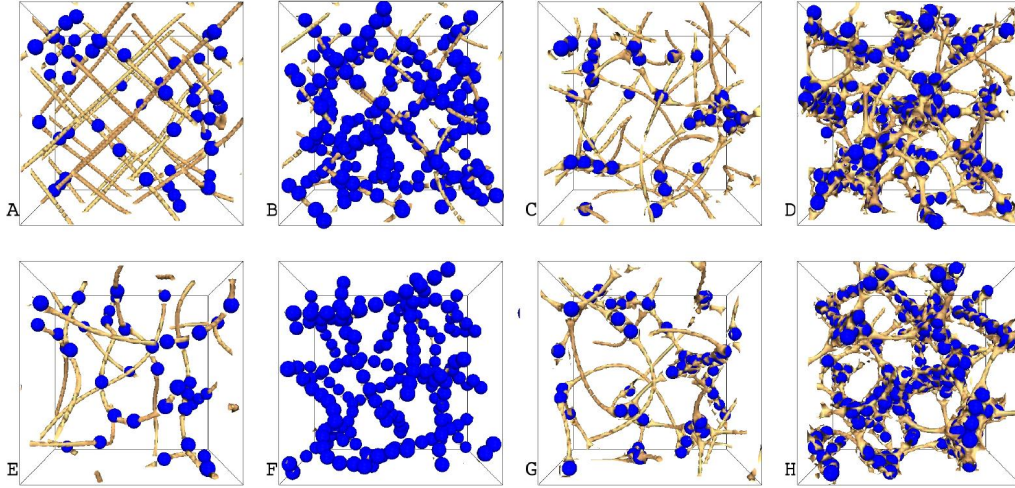


Figure 1: **Bulk blue phase structures.** Snapshots of the states obtained after dispersing a suspension of colloidal nanoparticles within a cholesteric liquid crystal in the BPI-forming region. (a)–(d) correspond to the case of a dispersion of particles in a pre-equilibrated BPI phase; (e)–(h) are obtained by dispersing colloids in an isotropic phase and then quenching into the range where BPI is stable, leading to formation of an amorphous, BPIII-like, disclination network. Structures correspond to: (a) and (e) $w = 0.23$ and $\phi = 1\%$; (b) and (f) $w = 0.23$ and $\phi = 5\%$; (c) and (g) $w = 2.3$ and $\phi = 1\%$; (d) and (h) $w = 2.3$ and $\phi = 5\%$. The anchoring of the director field to the colloidal surface is normal. [For the full parameter list used to generate Figs. 1-3 see Supplementary Notes.] For clarity, only a portion of the simulation box is shown its linear extent being $\simeq 28R$ (one eighth of the total volume); the full structures are shown in Supplementary Figs. 2 and 3.

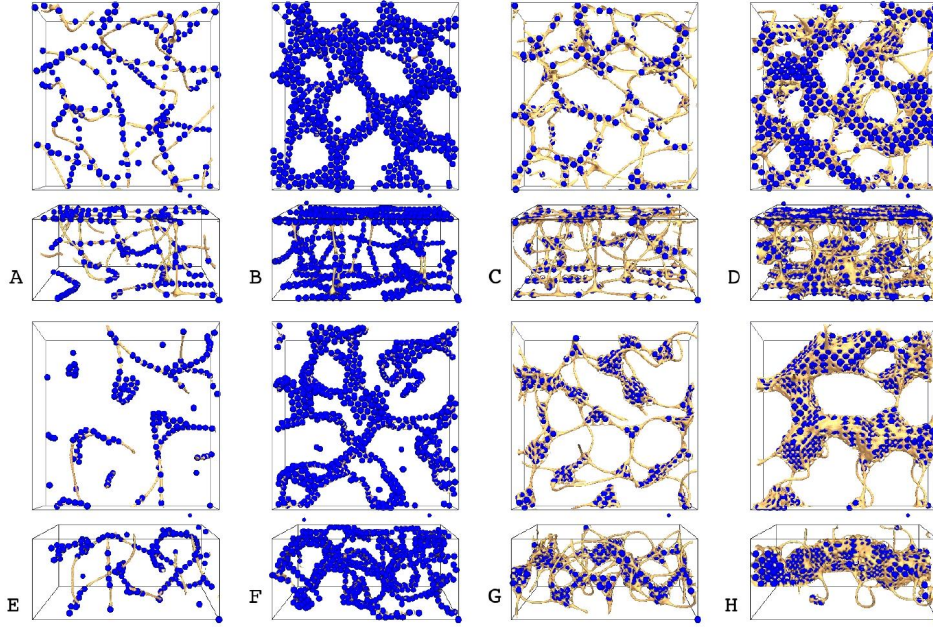


Figure 2: **Confined blue phase structures.** Snapshots of the steady states obtained when a dispersion of colloids in the isotropic phase is placed in a sandwich geometry, and then quenched into a regime where BPI is stable in the bulk. Both top and side views are provided. The anchoring of the director field at the walls is normal for (a)–(d) and planar for (e)–(h). Structures correspond to: (a) and (e) $w = 0.23$ and $\phi = 1\%$; (b) and (f) $w = 0.23$ and $\phi = 2\%$; (c) and (g) $w = 2.3$ and $\phi = 1\%$; (d) and (h) $w = 2.3$ and $\phi = 2\%$. As in Fig. 1, only one quarter of the simulation box is shown for clarity (its horizontal extent being $\simeq 56R$ and vertical extent $\simeq 24R$ in the narrow direction); the full structures are shown in Supplementary Figs. 5 and 6.

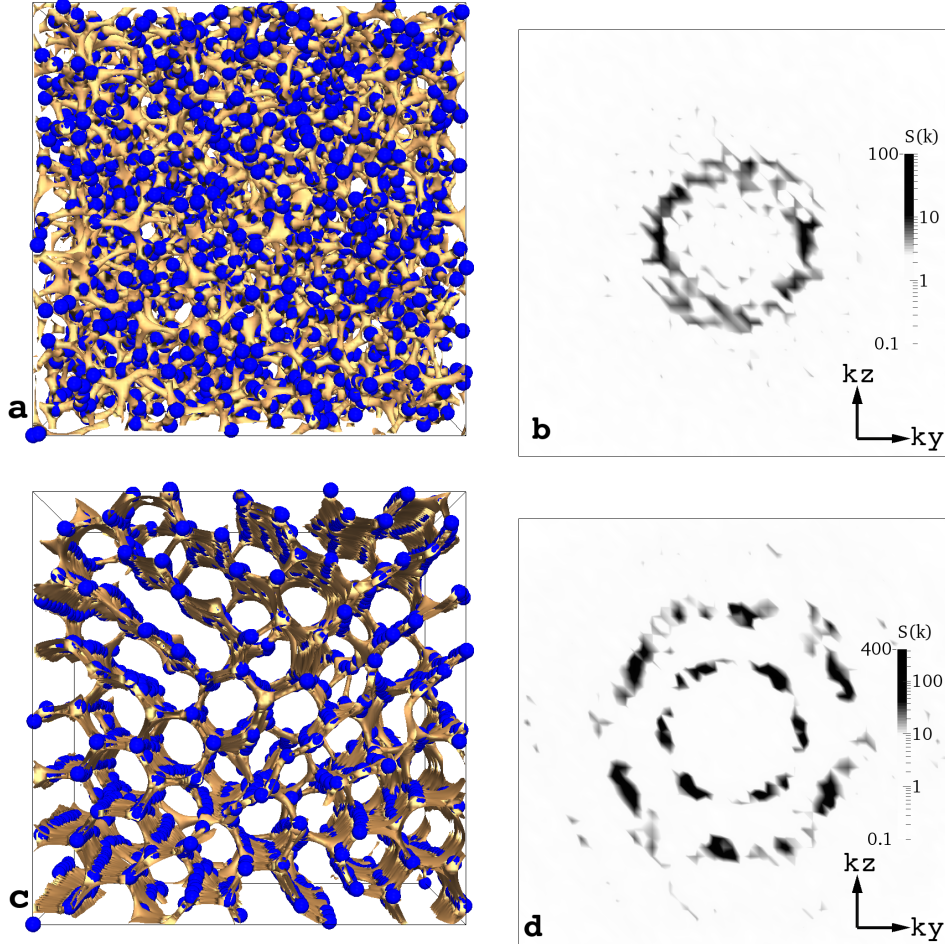
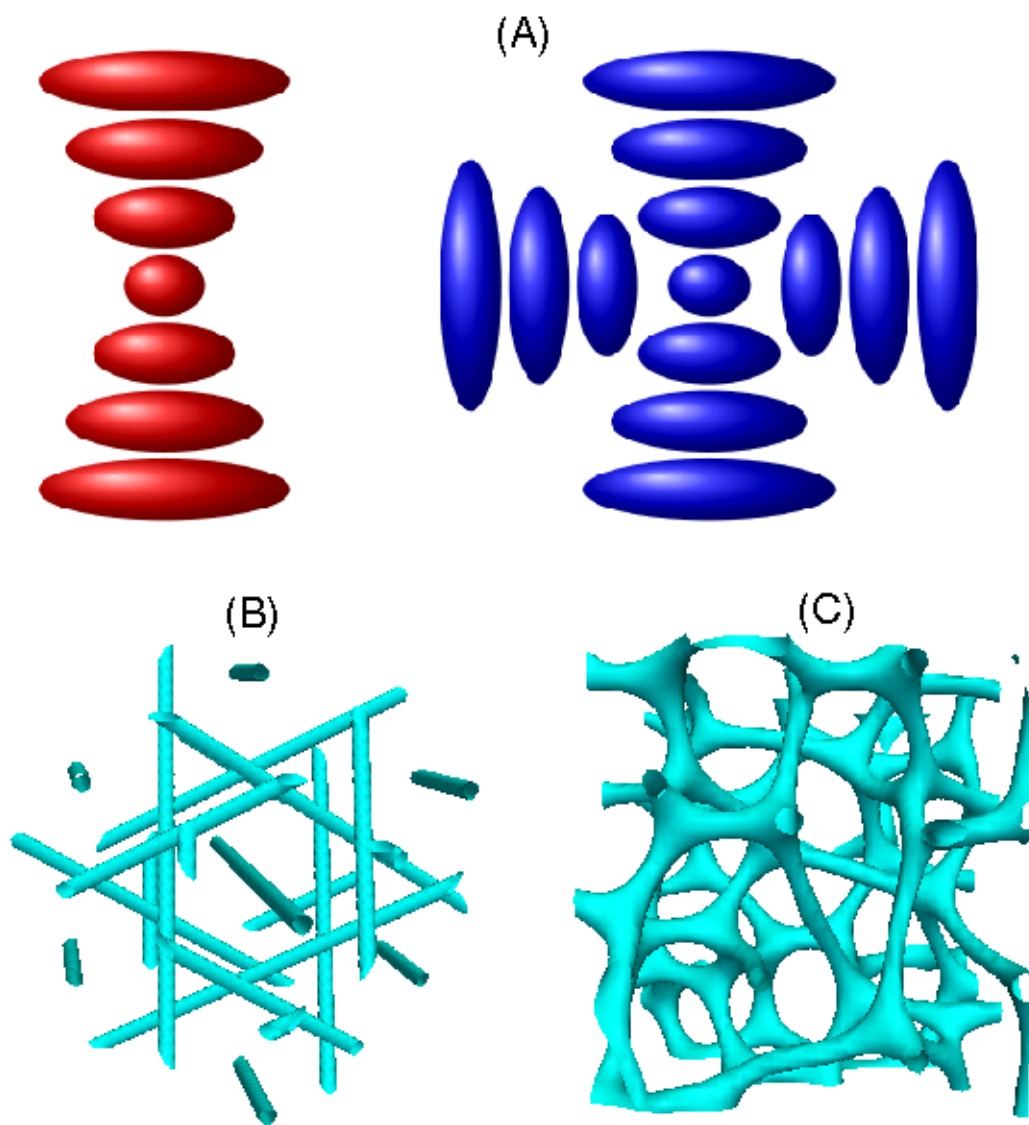


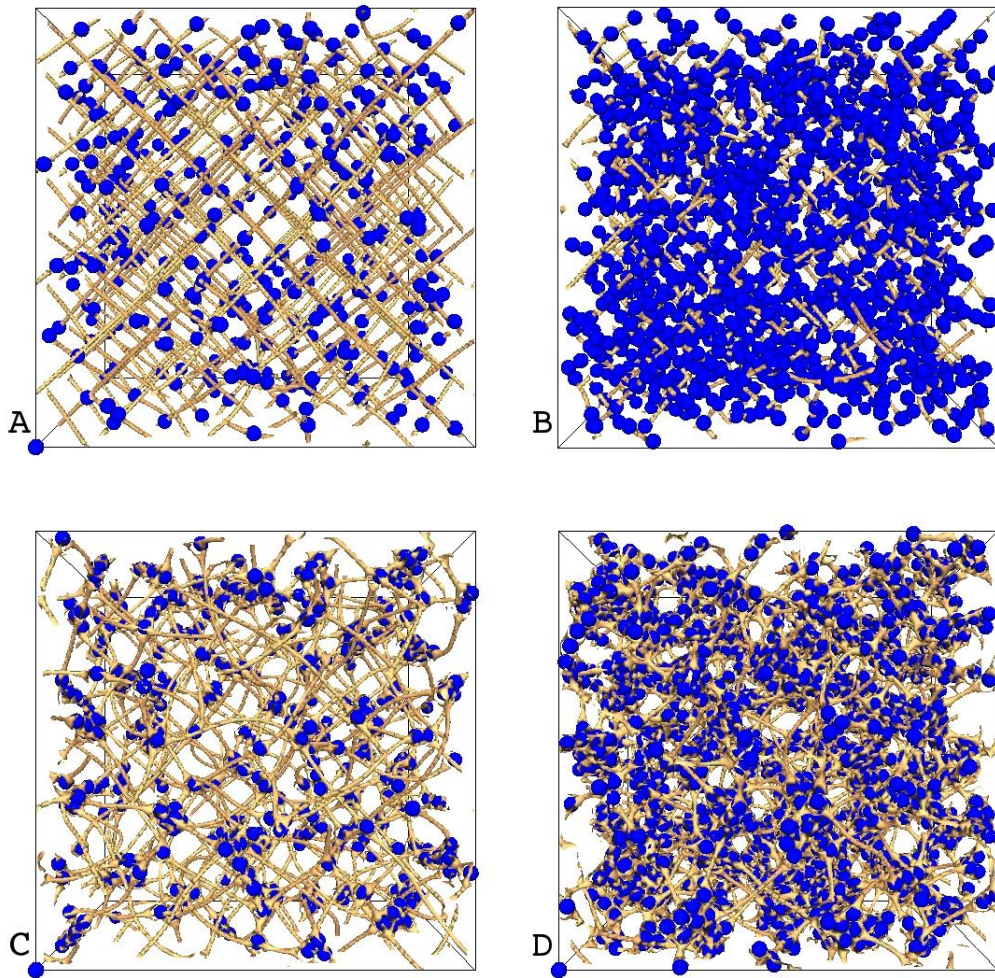
Figure 3: **Structure in electric field.** Steady states obtained when a dispersion of colloids is inserted into a thermodynamically stable bulk BPIII with and without applied external electric field. Panel (a) shows the situation in zero field, and panel (c) the situation when the applied field is in the x -direction (perpendicular to the plane of the paper). Panels (b) and (d) show one plane of the three-dimensional structure factor $S(\mathbf{k})$ computed from the positions of the particles, with wavevector $k_x = 0$, corresponding to (a) and (c) respectively. With field, the disclinations form a honeycomb pattern with hexagonal ordering perpendicular to the field direction; this is reflected in the structure factor. Simulations use weakly anchoring particles $w = 0.23$, and a volume fraction of $\phi = 5\%$ (see Supplementary Notes for full list of parameters). The full simulation with a box size of $\simeq 56R$ is shown.

Blank page.

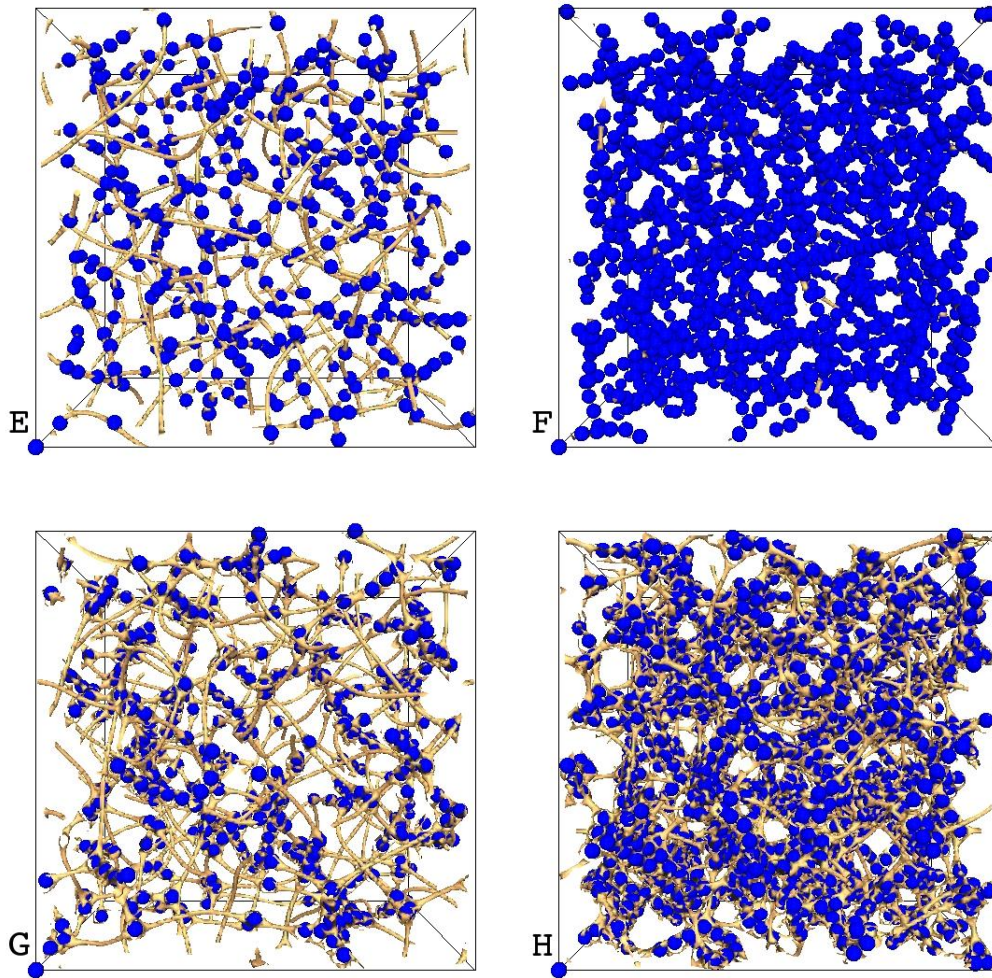
Supplementary Figures



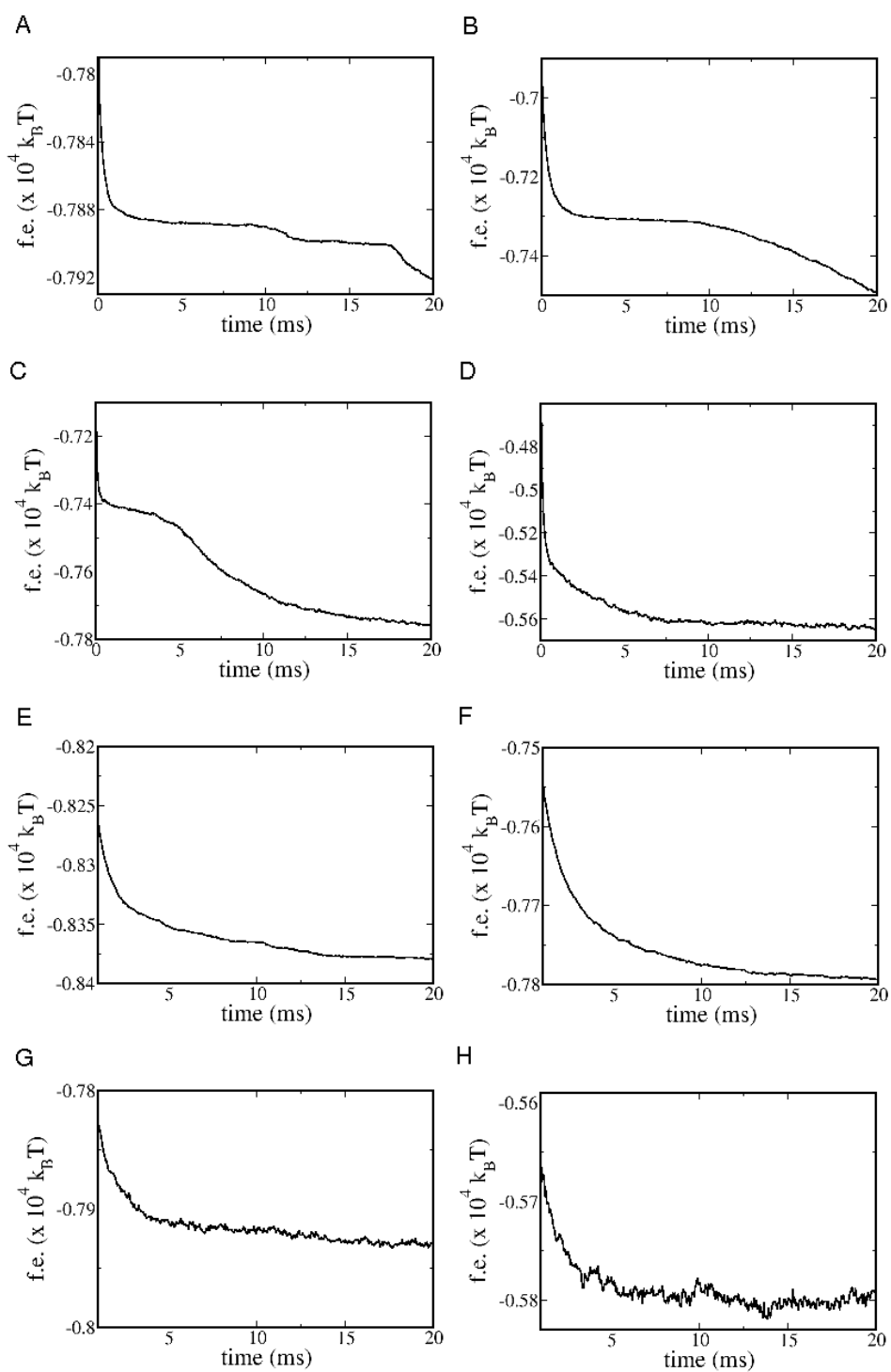
Supplementary Figure 4: **Blue phase structures.** (A) Schematic representation of the director field in a cholesteric (left) and within a double twist cylinder (right). (B) Snapshot of the disclination network in an equilibrated blue phase I structure. (C) Same as (B) for an amorphous blue phase III network.



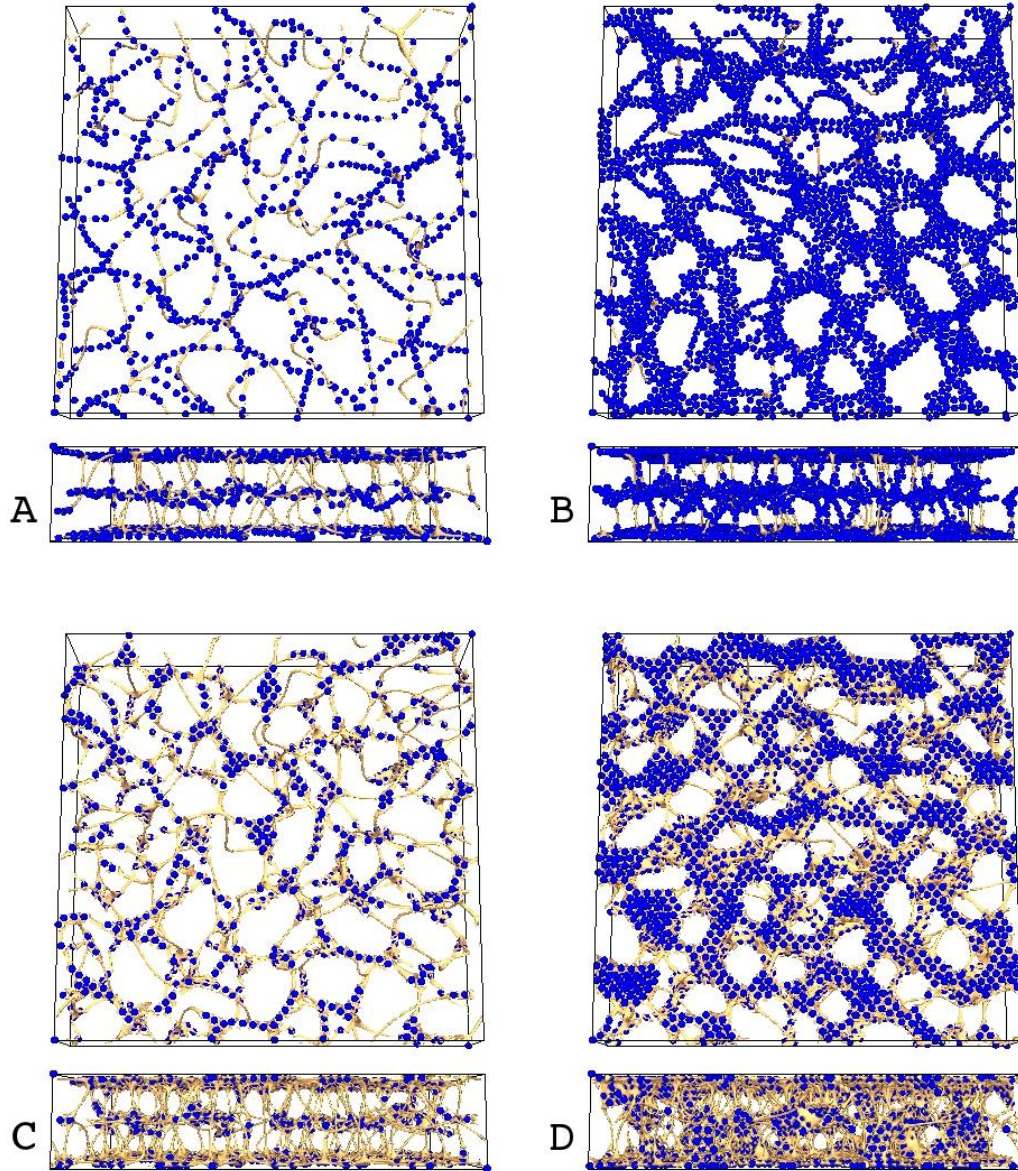
Supplementary Figure 5: **Bulk blue phase structures.** As for main manuscript Fig. 1 **a-d** (with liquid crystal order parameter initialised to equilibrium blue phase I structure), but for the entire simulation system of 128^3 lattice sites. (A) solid volume fraction 1% and weak anchoring; (B) 4% solid volume fraction and weak anchoring; (C) 1% solid volume fraction and strong anchoring; (D) 4% solid volume fraction and strong anchoring. The view direction in the main figure is from the left here. There is a reference particle at the bottom left in each panel which does not take part in the simulation.



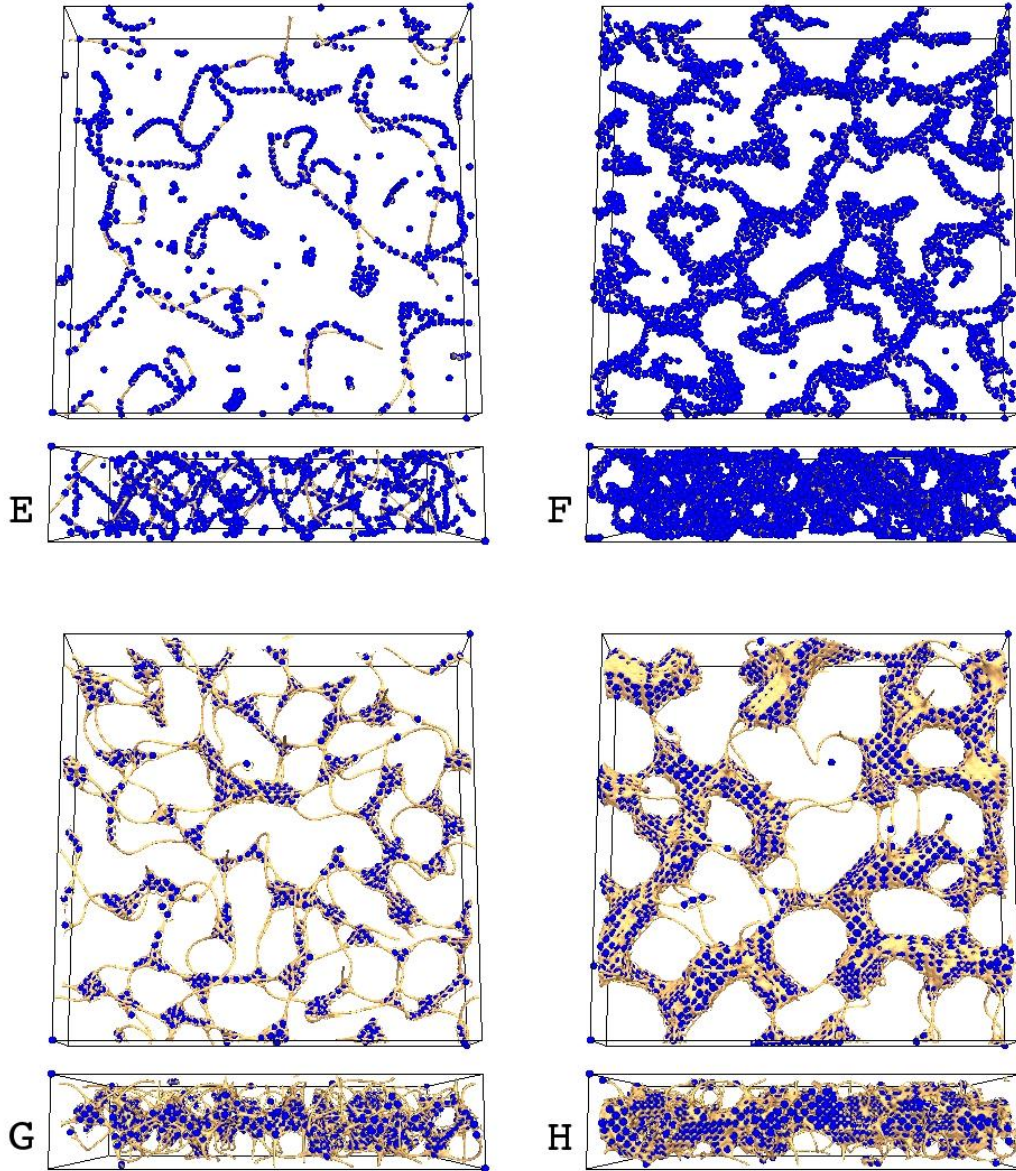
Supplementary Figure 6: **Bulk blue phase structures.** As for main manuscript Fig. 1 e–h (initialised via a “quench” to generate a disordered network), but for the entire simulation system of 128^3 lattice sites. (E) solid volume fraction 1% and weak anchoring; (F) 4% solid volume fraction and weak anchoring; (G) 1% solid volume fraction and strong anchoring; (H) 4% solid volume fraction and strong anchoring. Again, there is a reference particle at the bottom left in each case which does not take part in the simulation.



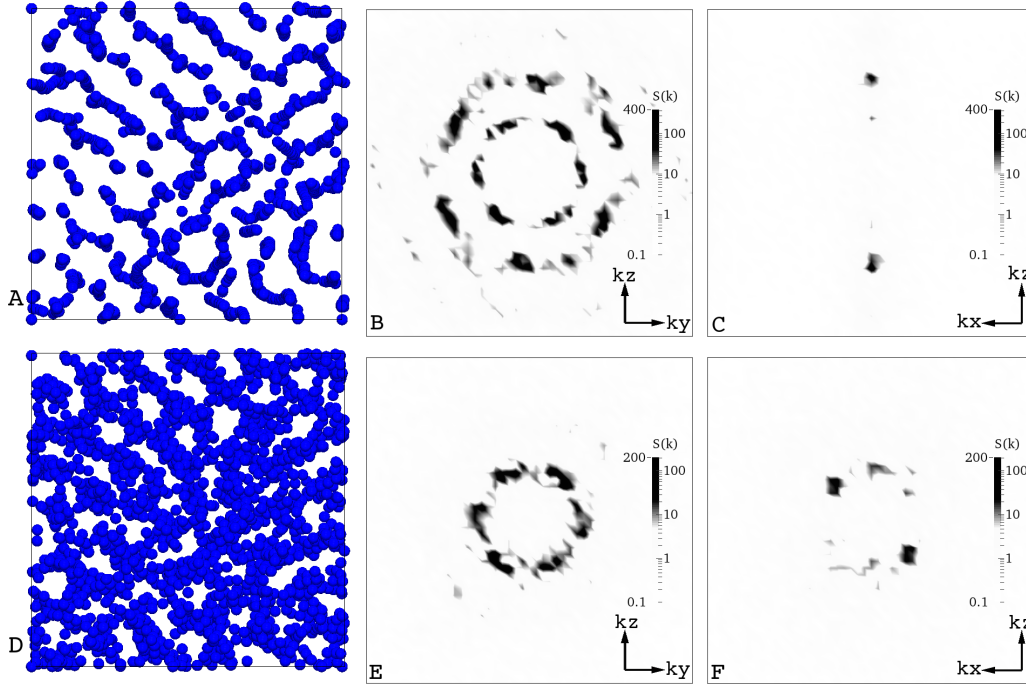
Supplementary Figure 7: **Free energy evolution.** Plot of the free energy (per BP unit cell) versus time for the simulations corresponding to Fig. 1 (a–h) in the main text.



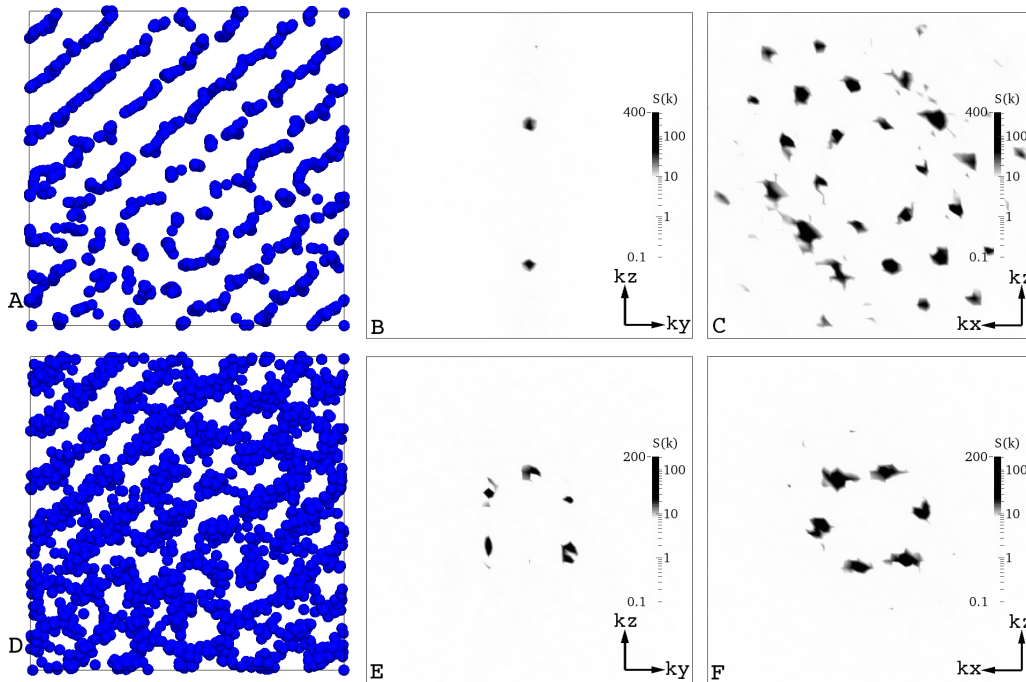
Supplementary Figure 8: **Confined blue phase structures.** As for main manuscript Fig. 2 **a–d** (confined geometry with normal anchoring walls at both top and bottom), but for the entire simulation system of $256^2 \times 56$ lattice sites. Each shows a top view and side view of the same simulation state. (A) solid volume fraction 1% and weak anchoring; (B) 4% solid volume fraction and weak anchoring; (C) 1% solid volume fraction and strong anchoring; (D) 4% solid volume fraction and strong anchoring.



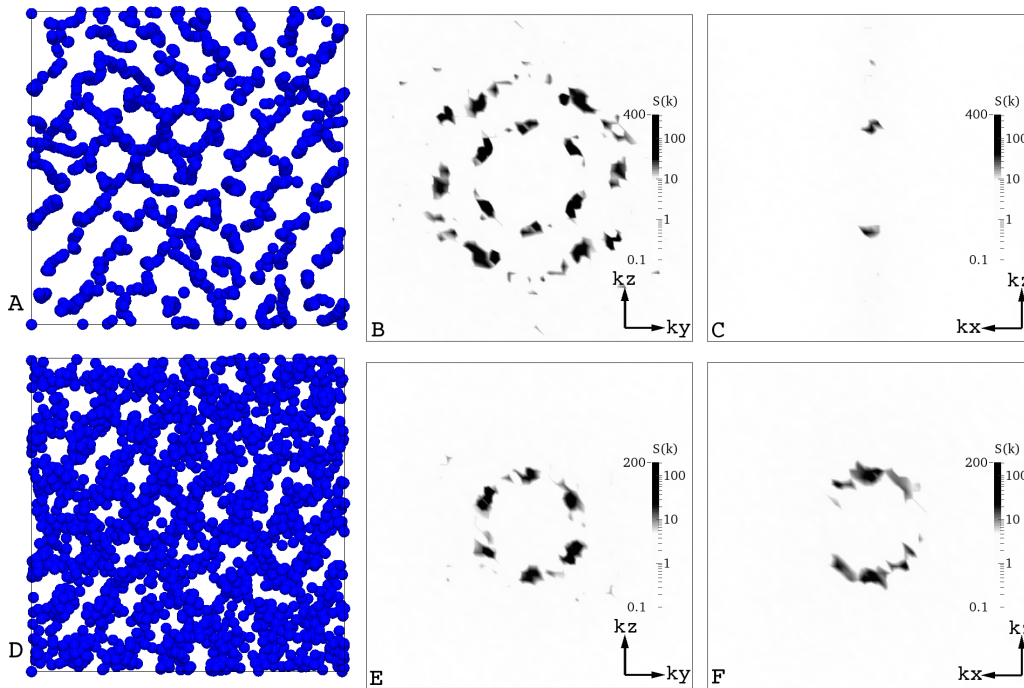
Supplementary Figure 9: **Confined blue phase structures.** As for main manuscript Fig. 2 e–h (confined geometry with planar anchoring walls at both top and bottom), but for the entire simulation system of $256^2 \times 56$ lattice sites. Each shows a top view and side view of the same simulation state. (E) colloid solid volume fraction 1% and weak anchoring; (F) 4% solid volume fraction and weak anchoring; (G) 1% solid volume fraction and strong anchoring; (H) 4% solid volume fraction and strong anchoring.



Supplementary Figure 10: **Structure with and without electric field.** (Disclination lines are removed for clarity.) Panels A and B reproduce the results in Fig. 3c and Fig. 3d respectively with the applied field in the x -direction (out of the plane of the paper). Also included is a cut of the structure factor with $k_y = 0$ (panel C). Panels D, E, and F show the corresponding situation after the external field has been removed and the structure allowed to relax, and show residual hexagonal ordering. The structure factor data is for wave vectors $k_x = 0; (k_y, k_z) \in [-3\pi/8, 3\pi/8]$ (panels B and E) and $k_y = 0; (k_x, k_z) \in [-3\pi/8, 3\pi/8]$ (panels C and F).



Supplementary Figure 11: **Cycling the electric field.** Starting from the final position of Supplementary Fig. 7 panel D, the field is re-applied, this time in the y -direction. The corresponding view of the particle distribution is shown, again viewing along the field direction, in panel A. Corresponding structure factor cuts with $k_x = 0$ and $k_y = 0$ are shown in panels B and C, respectively. The corresponding situation when the field is again switched off, and the structure allowed to relax, is shown in panels D, E, and F. The wave vector values used are the same as in Supplementary Fig. 7.



Supplementary Figure 12: **Cycling the electric field further.** Starting from the final position of Supplementary Fig. 8 panel D, the field is re-applied again in the x -direction. Panel A shows the particle configuration viewed along the field direction, and panels B and C show the structure factor with $k_x = 0$ and $k_y = 0$ respectively. The corresponding situation when the field is removed and the structure allowed to relax is shown in panels D, E, and F. The wave vector values are again as in Supplementary Fig. 7. Note that the on and off states are equivalent to those in Supplementary Fig. 7, up to a rotation. This is because all hexagonal structures perpendicular to the field direction are energetically degenerate, and the actual orientation of the hexagon emerges spontaneously during switching.

Supplementary Table

| | A_0 | γ | K | p | κ | τ | WR/K |
|----------------|-------|----------|----------|--------------|----------|---------|-----------|
| Bulk BPI | 0.01 | 3.086 | 0.007061 | $32\sqrt{2}$ | 0.6902 | -0.2500 | 0.23, 2.3 |
| Bulk Quench | 0.01 | 3.086 | 0.007061 | $32\sqrt{2}$ | 0.6902 | -0.2500 | 0.23, 2.3 |
| Confined | 0.01 | 3.086 | 0.01897 | 64 | 0.8 | -0.2500 | 0.23, 2.3 |
| External field | 0.004 | 3.086 | 0.02 | 32 | 2.6 | -0.2500 | 0.23 |

Supplementary Table 1: **Free energy parameters used in the simulations.** Bulk BPI correspond to Fig. 1 (a–d), bulk quench to Fig. 1 (e–h); confined geometries are shown in Fig. 2; and the external field case is relevant for Fig. 3.

Supplementary Methods

Parameter details for bulk BPI. The parameters for the free energy are chosen to be representative of blue phase I: chirality $\kappa \sim 0.7$ and reduced temperature $\tau = -0.25$. The full free energy parameters are shown in Table 1. The order parameter tensor $Q_{\alpha\beta}$ for bulk blue phase I is initialised from an approximation in high chirality limit [1, 2]. Systems of 128^3 lattice sites are used with a pitch length of $p = 32\sqrt{2}$, which accommodates 4^3 unit cells with fully periodic boundary conditions. Simulations at different solid volume fractions (1% and 4%), and different surface anchoring strengths ($WR/K = 0.23$ and $WR/K = 2.3$) representing “weak” and “strong” anchoring are run for two million simulation time steps. The initial distribution of the colloid positions is set at random for the required solid volume fraction; the colloids are initially at rest.

To generate a disordered network of disclination lines, a “quench” is performed in which the order parameter is initialised via a locally chosen random director, and Eq. 15 employed with a small amplitude $q^0 = 10^{-7}$ to provide an order parameter. The mean-field spinodal point at $\gamma = 3.0$ is avoided and the parameters are the same as for the initial simulations with pitch $p = 32\sqrt{2}$. The chirality and reduced temperature (see Table 1) remain appropriate for BPI. Colloids are added as before and the simulations run for 2 million simulation steps.

For simplicity, the size of the BPI unit cell is not allowed to readjust dynamically to minimise free energy (there is no “redshift” [1]): this would lead to quantitatively different values of the free energy, but qualitatively similar structures.

Parameters for confined BPI. Here, a narrow sandwich of fluid is placed between flat walls in perpendicular to the narrow coordinate direction, and with periodic boundaries in the other two directions. The system size used in all cases is $256^2 \times 56$ lattice sites. Each simulation is a “quench” in a similar manner to that used in the bulk: the order parameter is initialised randomly. The free energy parameters (see Table 1) are again appropriate for (equilibrium) blue phase I (chirality $\kappa = 0.8$ and reduced temperature $\tau = -0.25$). The cholesteric pitch is set to be $p = 64$, providing a slightly better resolution than the bulk simulations.

The surface anchoring for colloids is as before: always normal, but with $WR/K = 0.23$ and $WR/K = 2.3$. The colloid solid volume fractions are 1% and 4%. For both normal and planar anchoring at the walls, the strength is adjusted to correspond to that used for the strongly anchoring particles. All simulations are run for two million simulation time steps.

External electric field. For the simulations of BPIII with colloidal particles a system size of 128^3 is used with a cholesteric pitch of $p = 32$ in lattice units. The simulations are performed at chirality $\kappa = 2.6$ and reduced temperature $\tau = -0.25$. An initial configuration of randomly oriented and positioned

double twist cylinders is used, from which an amorphous BPIII network emerges [3]. This structure is equilibrated for 6×10^5 LB time steps until no significant further evolution is observed.

The colloidal particles with weak normal anchoring ($WR/K = 0.23$), are then inserted with randomly chosen positions, and the composite system is equilibrated for another 1.2×10^6 time steps. At the end of the equilibration phase the uniform electric field with reduced field strength $\mathcal{E} = 0.8$ is switched on (oriented along the z -direction), and the simulation run for a further 1.2×10^6 time steps. This is found to be sufficiently long for a hexagonal structure to emerge and saturate. If the electric field is then switched off, and the system quickly relaxes to a metastable state which shows a residual anisotropy in the colloidal distribution. The total length of this final relaxation phase is 1×10^6 LB time steps.

Disclination rendering. In all cases visualisation of the defect lines is carried out via an isosurface of the scalar order parameter q determined from the largest eigenvalue of the local order parameter tensor. A low value of the scalar order parameter q (typically in the range 0.12–0.14) unambiguously identifies the disclinations.

Computation of the structure factor. To provide structural information about the field-aligned states and the residual anisotropy after switch off a procedure similar to the one described in [3] is followed. The structure factor $S(\mathbf{k})$ in the current approach is defined via the Fourier transform of the colloid density $F(\mathbf{k})$:

$$S(\mathbf{k}) = |F(\mathbf{k})|^2, \text{ with } F(\mathbf{k}) = \int d^3\mathbf{r} \rho(\mathbf{r}) e^{i\mathbf{k}\cdot\mathbf{r}}. \quad (17)$$

The colloid density $\rho(\mathbf{r})$ is a discretised density and taken to be $\rho(\mathbf{r}) = 1$ if a lattice site at \mathbf{r} is part of a colloid and $\rho(\mathbf{r}) = 0$ otherwise. This definition, which deviates from the standard definition of a structure factor and does not consider the colloids as point-like objects, allows the same structural information to be obtained in a simple way.

Parameter mapping to physical units. To get from simulation to physical units, a calibration of scales of length, energy and time in the simulations is required. For similar mappings see, e.g. [4].

The length scale can be set by mapping the half pitch to a realistic blue phase unit cell size, which is in the 100–500 nm range [1]. For bulk simulations (Fig. 1 and Fig. 3 in the main text), a suitable choice is one where one simulation unit (lattice site) corresponds to 10 nm. Therefore the colloidal size in Figs. 1 and 3 corresponds to ~ 50 nm.

To obtain an energy scale, it is possible to choose $A_0 \simeq 10^6$ Pa, which is reasonable following Ref. [1] (this is also the choice in Ref. [5]). This choice leads to a simulation unit of free energy (or stress) equal to 10^8 Pa in Figs. 1 and 3. From the energy and length scales one can map elastic constants to

physical units: for instance, the simulation in Fig. 1 corresponds to a liquid crystal with splay, bend and twist (Frank) elastic constants equal to 35 pN (or equivalently $K = 70$ pN).

The timescale calibration may be obtained from (see e.g. [6])

$$\gamma_1 = \frac{2q^2}{\Gamma}, \quad (18)$$

which relates the rotational viscosity γ_1 to the ordering strength q and the order parameter mobility Γ . In the present simulations, $\Gamma = 0.5$ and the value of γ for the simulation in Fig. 1 leads to $q = 1/2$. For real liquid crystalline materials, γ_1 usually lies in range $10^{-2} - 1$ Pa s [7]; for definiteness say $\gamma_1 = 1$ Pa s (equivalently 10 poise). Given the previous mapping for free energy (or stress) units, this leads to a simulation unit of time equal to 10^{-8} s. The total simulated time in Figs. 1-3 is therefore in the millisecond range.

To calibrate the electric field strength one can equate the value of the dimensionless parameter \mathcal{E} in the simulations with that of a hypothetical experiment. Given the previous value for A_0 , and a dielectric anisotropy of 20 (or equivalently $\epsilon_a = 20\epsilon_0$, with ϵ_0 the dielectric permittivity of vacuum), an electric field of $100 \text{ V } \mu\text{m}^{-1}$ is obtained. This corresponds to a value of $\mathcal{E} \sim 0.4$ (considering a value of $\gamma = 3.0857$ as in Fig. 3 of the main text).

Given these mappings, all quantities can be easily transformed from simulation to physical units and vice versa. For example Figs. 1 and 2 use an isotropic viscosity $\eta \simeq 0.01$ and 0.1 in simulation units, which translate into $0.01 - 0.1$ Pa s respectively. This is sensible (if slightly low) for a molecular nematogen in the isotropic phase. The effective viscosity in ordered phases is higher, but this is ensured in our model by the coupling to the order parameter. Note that the density is set to unity in the simulations: this corresponds to a fluid density which is about a thousand times larger than in experiments. This makes no difference in practice as the Reynolds number $= \rho V \Lambda / \eta$ (where V is a typical velocity, in our simulations around 10^{-5} in lattice units, and Λ is a typical length scale, e.g. the size of a unit cell) remains small enough [8].

To summarise, the simulations represent BP-forming materials, with the interpretation of the simulation units for length, time, and energy density being close to 10 nm, 10 ns, and 100 MPa respectively. For a Frank elastic constant of $K = 70$ pN and unit cell sizes in the range $\lambda = 100 - 500$ nm, a corresponding shear modulus $G \simeq K/\lambda^2 = 0.3 - 7$ kPa.

Supplementary References

- [1] Wright, D.C., and Mermin, N.D., Crystalline liquids: the blue phases, *Rev. Mod. Phys.* **61**, 385-432 (1989).
- [2] Henrich, O., Marenduzzo, D., Stratford, K., and Cates, M.E., Thermodynamics of blue phases in electric fields, *Phys. Rev. E*, **81** 031706 (2010).
- [3] Henrich, O., Stratford, K., Cates, M.E., and Marenduzzo, D., Structure of blue phase III of cholesteric liquid crystals, *Phys. Rev. Lett.* **106**, 107802 (2011).
- [4] Denniston, C., Marenduzzo, D., Orlandini, E., and Yeomans, J.M., Lattice Boltzmann algorithm for three-dimensional liquid-crystal hydrodynamics, *Philos. Trans. R. Soc. London, Ser. A* **362**, 1745 (2004).
- [5] Henrich, O., Stratford, K., Marenduzzo, D., and Cates, M.E., Ordering dynamics of blue phases entails kinetic stabilization of amorphous networks, *Proc. Acad. Sci. USA* **107**, 1312 (2010).
- [6] Denniston, C., Orlandini, E., and Yeomans, J.M., Lattice Boltzmann simulations of liquid crystal hydrodynamics, *Phys. Rev. E* **63**, 056702 (2001).
- [7] de Gennes, P.-G., and Prost, J., *The Physics of Liquid Crystals* (Clarendon Press, 1995).
- [8] Cates, M.E., et al., Simulating colloid hydrodynamics with lattice Boltzmann, *J. Phys. Condens. Matter* **16**, 3903 (2004).